Applied Catalysis B: Environmental 154–155 (2014) 232–237

Contents lists available at ScienceDirect

Applied Catalysis B: Environmental

journal homepage: www.elsevier.com/locate/apcatb

Investigation of molybdenum carbide nano-rod as an efficient and durable electrocatalyst for hydrogen evolution in acidic and alkaline media

Peng Xiao [a], Ya Yan [a], Xiaoming Ge [b], Zhaolin Liu [b], Jing-Yuan Wang [c], Xin Wang [a,*]

[a] School of Chemical and Biomedical Engineering, Nanyang Technological University, 50 Nanyang Avenue, 639798 Singapore, Singapore
[b] Institute of Materials Research and Engineering (IMRE), Agency of Science, Technology, and Research (A*STAR), 3 Research Link, Singapore 117602, Singapore
[c] Residues and Resource Reclamation Centre, Nanyang Technological University, Singapore

ARTICLE INFO

Article history:
Received 9 November 2013
Received in revised form 29 January 2014
Accepted 11 February 2014
Available online 19 February 2014

Keywords:
Hydrogen evolution reaction
Molybdenum carbide
Nano-rod
Nickel impregnation
Electrocatalyst

ABSTRACT

A well-defined dimolybdenum carbide (Mo_2C) nano-rod with a porous structure is successfully synthesized through facile carburization of anilinium molybdate in hydrogen. As a catalyst for hydrogen evolution reaction (HER), we investigated its electrical conductivity and catalytic activity. It is found that, as a standalone catalyst, Mo_2C nano-rod shows a competitive performance for catalysing HER in acidic media. A composite catalyst based on Ni impregnated Mo_2C nano-rod is further synthesized to investigate its catalytic behaviour and reaction mechanism in alkaline condition. Compared to commercial Mo_2C, the enhanced performance of the Mo_2C nano-rod could be attributed to its porous structure with small particles as well as its high electrical conductivity.

1. Introduction

Hydrogen production from electrochemical splitting of water has attracted increasing interests because it can be realized using renewable energies [1]. Besides, the zero emission of carbonaceous species from hydrogen utilization makes hydrogen an ideal candidate for the replacement of fossil fuel energy in the future [2,3]. In the course of seeking highly efficient electrocatalysts for hydrogen production, Pt has emerged as the most efficient one in acidic media [4–7]. Unfortunately, the scarcity and high cost of Pt hinder its commercial application in large scale. In the past decades, efforts have been made to search for low-cost alternatives to reduce the use of Pt or even replace it [8]. Several non-noble metal based materials, such as transition-metal complexes [9,10], chalcogenides [11,12], carbide [13–15] and metal alloys [16] have been vigorously pursued as catalysts or supports for the electrochemical hydrogen evolution reaction (HER). Among them, molybdenum disulphide was highlighted as a superb and cost-effective catalyst [17–21], after polygonal molybdenum disulphide (MoS_2) nanocrystal with exposed edges on Au was found to be active towards HER [22,23] for the first time. However, apart from its instability in alkaline condition [13], the conductivity of MoS_2 is very low, ranging from *ca.* 10^{-8} S cm^{-1} [24] to 0.1 S cm^{-1} [25], which usually requires the additional incorporation of conductive substrates, such as graphene [26–28], carbon sphere [29], and carbon nanotubes [30].

Molybdenum carbide (Mo_2C), another type molybdenum compound, was widely employed as a catalyst for methane reforming [31], methanol steam reforming [32], oil conversion [33], water gas shift reaction [34], *etc.* Its electrochemical activity towards HER was only recently reported by Hu et al. [13,35]. Its derivatives, such as Mo_2C/CNT [36] and Mo_2C/RGO [37] also exhibit high activities towards hydrogen evolution. Catalytic activity and electrical conductivity are two critical factors for electrochemical applications. For Mo_2C, those two attributes have not been fully unveiled yet.

In this work, we synthesize Mo_2C nano-rods through a simple method of carburization of ammonium molybdate tetrahydrate and aniline complex [35,38,39]. A well-defined porous Mo_2C nano-rod with highly exposed (1 0 1) plane was obtained at 700 °C under 20% H_2/Ar, and the composition transformations during carburization process are carefully studied. The conductivity of the Mo_2C nano-rod pellet was measured using a four-probe method. The activities of molybdenum carbides towards HER were investigated in both acidic and alkaline media.

* Corresponding author. Tel.: +65 63168866; fax: +65 67947553.
E-mail address: WangXin@ntu.edu.sg (X. Wang).

http://dx.doi.org/10.1016/j.apcatb.2014.02.020
0926-3373/

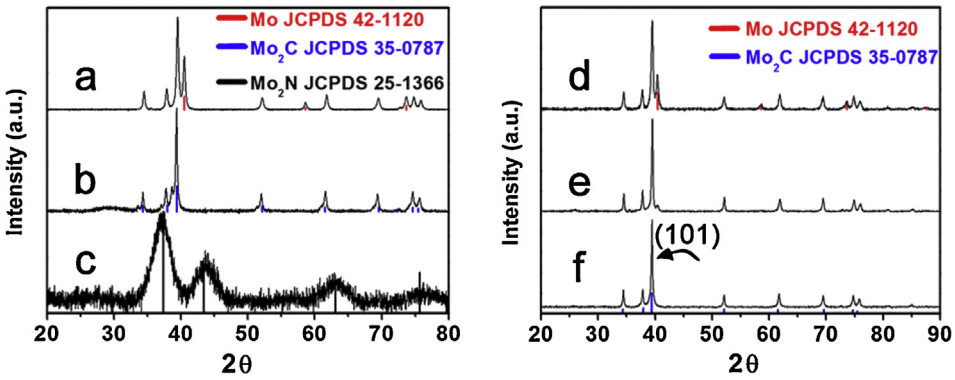

Fig. 1. XRD patterns of molybdates: (a) 700 °C, pure H_2; (b) 600 °C, pure H_2; (c) 450 °C, pure H_2; (d) 700 °C, 50 vol.% H_2/Ar; (e) 700 °C, 35 vol.% H_2/Ar; (f) 700 °C, 20 vol.% H_2/Ar.

2. Experimental

2.1. Mo_2C nano-rods synthesis

Ammonium molybdate tetrahydrate ($(NH_4)_6Mo_7O_{24}{\cdot}4H_2O$) (Sigma–Aldrich) was used as the Mo precursor. Aniline (Sigma–Aldrich, >98%) was used as received. In a typical procedure, 0.827 g $(NH_4)_6Mo_7O_{24}{\cdot}4H_2O$ was dissolved by 10 ml DI-water in a vial, and 1.089 ml aniline was pipetted into the solution. The pH value of the solution was adjusted to ~4.5 by stepwise dropping 1 M HCl under vigorous stirring. Finally, the obtained suspension in a vial was mounted in a water bathing receptacle at 80 °C for 3 h. After reaction, the yellowish product was washed by ethanol repeatedly. Before carburization, the as-synthesized Mo_2C nano-rod was dispersed into water for ultrasonication in a 15 s-on–15 s-off mode for 1 h and dried at 80 °C overnight. Carburization experiments were carried out at different temperatures (450–700 °C) in various gas compositions. Nickel was loaded onto Mo_2C rod by impregnation of 1 M $Ni(NO_3)_2$ and post-sintered at 450 °C under reducing conditions.

2.2. Material characterization

X-ray diffraction (XRD) was conducted using a Cu Kα radiation source (Bruker, Japan) to examine the phase structures after carburization. Morphological contrasts were observed by using a field emission scanning electron microscope (FE-SEM, JEOL, JSM6701F, Japan) while transmission electron microscopy (TEM) and high resolution TEM images were collected on TEM Philips CM300. Raman spectroscopy spectrum was measured by a laser of 514 nm wavelength on the as-synthesized Mo_2C nano-rod. X-ray photoelectron spectroscopy (XPS) was performed on a VG Escalab 200i-XL spectrometer equipped with a monochromatic Al Kα (1486.6 eV) X-ray source. The electrical conductivity tests were conducted using a four-probe method on a thin rectangular bar of dimensions 24 mm × 5 mm × 1 mm, which was uni-axially die-pressed under 300 MPa. Both electrochemical impedance spectroscopy (EIS) and linear scanning voltammetry were applied to measure the conductivity. Polarization curves of the HER were collected by an Autolab PGSTAT302/FRA system (Eco Chemie, Netherland) in a three-electrode configuration at room temperature and Pt foil and saturated calomel electrode (SCE) were used as the auxiliary electrode and the reference electrode, respectively. Firstly, SCE was calibrated by using Pt foil as the working electrode both in 0.5 M H_2SO_4 and 1 M KOH solution (see Figs. S1 and S2) that was purged by N_2 for half an hour before the tests. Thus, all the potentials were recorded with respect to the reversible hydrogen electrode (RHE). Catalyst ink was typically made by dispersing 3.5 mg of catalyst in 2 ml ethanol. After adding 0.5 ml of 0.05 wt.% of Nafion solution (Gashub, Singapore) and ultrasonication, a certain amount of black slurry was pipetted onto the glassy carbon electrode (0.1963 cm^2). Current density was normalized to the geometrical area of the working electrode. Electrochemical impedance spectroscopy (EIS) was conducted in a potentiostatic mode in the frequency range of 10^5–0.1 Hz with a perturbation of 10 mV. At different overpotentials (η = 0–200 mV), EIS curves were recorded. In particular, at η = 200 mV, the obtained impedances were fitted by the Zview program. Tafel plots were drawn after *IR* compensation *i.e.* $\eta_{cor} = \eta - jR_{cor} = a + b \ln j$, where η (V) denotes the experimental potential applied *vs.* RHE, η_{cor} (V) as the *IR* compensated potential, b (mV dec^{-1}) as the Tafel slope, j (mA cm^{-2}) as the normalized current density, and R_{cor} can be obtained from Nyquist plot.

3. Results and discussion

3.1. Phase transition from molybdenum complex to Mo_2C nano-rod and its morphology

Through a self-assembly method to attach protonated aniline to trimolybdate anions [40,41], anisotropic growth [39] of anilinium trimolybdate forms 1D nano-rods at 80 °C. The as-prepared precursor was firstly annealed in pure H_2 for 1 h at the temperature ranging from 450 °C to 700 °C. The corresponding XRD patterns are shown in Fig. 1. At 450 °C, Mo_2N phase is observed (Fig. 1c), but the crystallinity is fairly low and the calculated particle size is ~3.4 nm from the Scherrer's equation. When the temperature is raised up to 600 °C, Mo_2C phase emerges as shown in Fig. 1b, but a hump of an unknown impurity at around 30° can be discerned. With the further increase of temperature to 700 °C (Fig. 1a), Mo_2C phase (JCPDS 35-0787) stands out, but a new peak emerges at 40.5° that is indexed to metallic Mo. Hence, 50 vol.%, 35 vol.% and 20 vol.% of H_2 balanced by argon are fed, and lead to a decreased content of Mo in Mo_2C accordingly as shown in Fig. 1d–f. To be specific, the Mo_2C obtained in 50 vol.% H_2/Ar and 35 vol.% H_2/Ar are denoted HMo-Mo_2C-R, LMo-Mo_2C-R, respectively, whereas the samples obtained in 20 vol.% H_2/Ar show no diffraction signal of metallic Mo and are named as Mo_2C-R. Then FE-SEM was employed to examine the morphology contrast among HMo-Mo_2C-R, LMo-Mo_2C-R and Mo_2C-R. Clearly, both HMo-Mo_2C-R and LMo-Mo_2C-R show rough surfaces embedded with small particles (Fig. S3), and XRD patterns suggest that those particles should be metallic Mo, corresponding to the peak emerging at 40.5° in Fig. 1(a, d, e). In sharp contrast, Mo_2C-R exhibits smooth surface with a rod diameter of ~50 nm to ~200 nm in Fig. 2a.

TEM images shown in Fig. 2b reveal a porous structure of the synthesized Mo_2C nano-rods, consistent with a previous study [35,38]. N_2 adsorption/desorption renders a BET specific surface

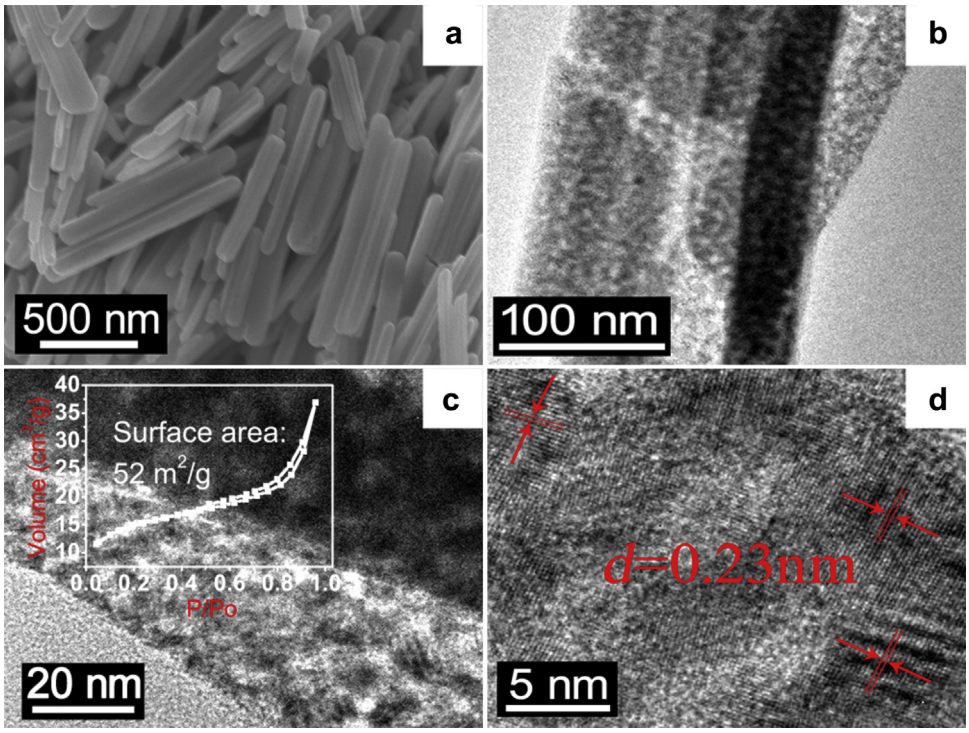

Fig. 2. Morphology of Mo_2C-R (a) FESEM images; (b–d) TEM images.

area of 52 m^2/g (the inset graph of Fig. 2c). Considering the size of nano-rod (50–200 nm), it is hard to achieve a high surface area if it is compact. On the contrary, it underpins the fact that Mo_2C nano-rods could be porous, in accordance with what we observed though TEM. Further magnified graph of TEM in Fig. 2c presents the interconnected particles, with groups of parallel lines on some particles. Fig. 2d suggests that those lines are arrayed with (1 0 1) plane of Mo_2C with a *d*-space of 0.23 nm, corresponding to the diffraction peak observed by XRD (Fig. 1f).

X-ray photoelectron spectroscopy (XPS) was employed to further elucidate the composition of Mo_2C-R. HMo-Mo_2C-R was also examined for the purpose of comparison. As shown in Fig. 3, both deconvoluted profiles of Mo_2C-R and HMo-Mo_2C-R show MoO_3 and MoO_2 [13,42,43], suggesting that Mo_2C is prone to oxidation on the surface. Fig. 3b also reveals that HMo-Mo_2C-R includes a doublet of 227.7 eV/230.8 eV, which can be ascribed to the metallic Mo decorated on Mo_2C, while no metallic Mo is observed on Mo_2C-R sample, in accordance with XRD results.

3.2. Electrochemical, conductivity test

Before the measurement of conductivity, Raman spectroscopy experiments were conducted for further confirmation of the residue carbon that the as-prepared Mo_2C-R may retain during carburization. As shown in Fig. 4, no characteristic peaks, *e.g.* the D band, G band or 2D band [44,45] of carbon materials are detected, instead it only manifests typical peaks of Mo_2C [46]. The electrical conductivity of Mo_2C is critical for electrocatalytic application and was measured at room temperature. The results from both EIS and *I–V* measurement agree with each other quite well, rendering 30 S cm^{-1} (Fig. S4). This value is comparable to those commonly used substrates, such as RGO, which has a reported range of 0.5–100 S cm^{-1} [44,47]. It is noteworthy that the conductivity test may not fully exhibit its theoretical value as the die-pressed Mo_2C-R bar is still porous, which definitely underestimates its conductivity [48,49]. This indicates that Mo_2C nano-rod itself has sufficient conductivity for electrocatalytic application.

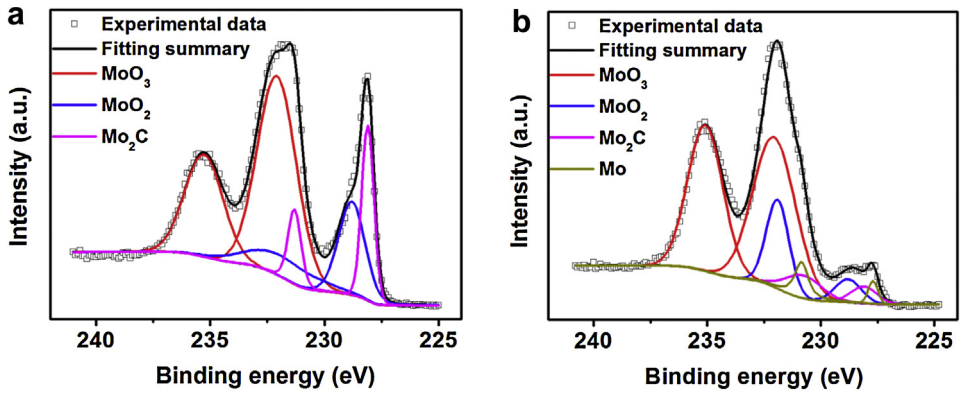

Fig. 3. XPS of (a) Mo_2C-R and (b) HMo-Mo_2C-R.

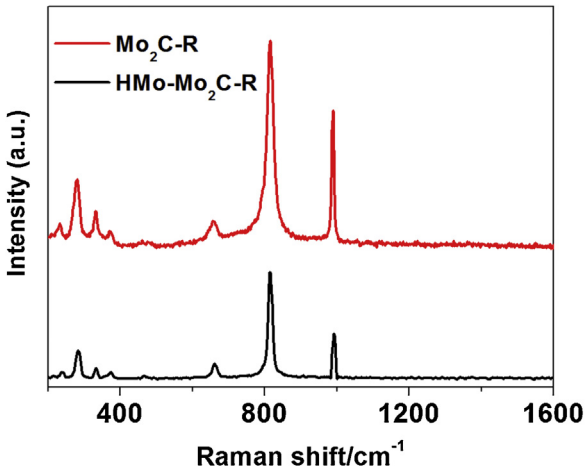

Fig. 4. Raman spectrum of Mo_2C-R and HMo-Mo_2C-R.

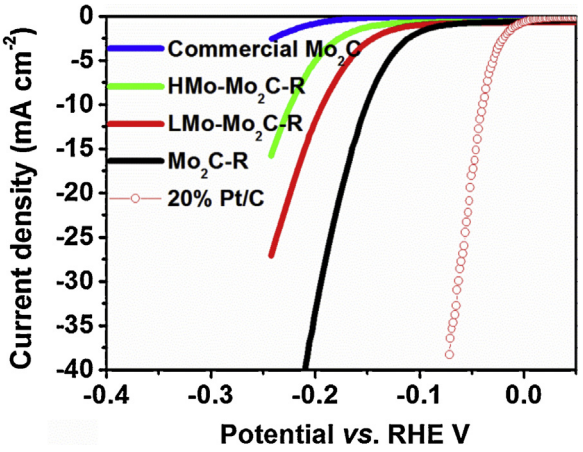

Fig. 5. Polarization curves in 0.5 M H_2SO_4, mass loading 0.43 mg cm^{-2}.

In a three-electrode configuration, linear scan voltammetry (LSV) experiments were firstly conducted in 0.5 M H_2SO_4. As shown in Fig. 5, all the as-synthesized Mo_2C nano-rods outperform commercial Mo_2C, and among them, Mo_2C-R exhibits the highest catalytic activity. The onset potentials for HMo-Mo_2C-R, LMo-Mo_2C-R and Mo_2C-R can be discerned as 125 mV, 97 mV and 68 mV, respectively, which are determined by reading the deviating point in the potential-log |*j*| plot (Fig. S5) [4,28]. For Mo_2C-R, the potential of $\eta = 200$ mV drives current densities of 32 mA cm^{-2} *vs.* 0.8 mA cm^{-2} for commercial Mo_2C, suggesting that it is a promising candidate as hydrogen evolution catalyst. Compared to commercial Mo_2C, this high performance is benefitted from small particulates among the porous structures observed in TEM images (Fig. 2) as this porous structure potentially increases the accessibility of protons to the inner particles. Interestingly, among the as-synthesized Mo_2C nano-rods, the cathodic current drops at the same applied potential with the increased content of metallic Mo in the catalysts. This phenomenon strongly indicates that metallic Mo is detrimental to the hydrogen evolution reaction. A theoretical calculation [11,50] of the binding energy of metallic Mo implies that metal Mo is not a good candidate for hydrogen evolution because of its strong bond to atomic H. Likewise, a slow H release caused by the strong hydrogen bond could explain the inferior performance of HMo-Mo_2C-R and LMo-Mo_2C-R to Mo_2C-R. Furthermore, the XPS spectra deconvolution shows that the carbide peak of HMo-Mo_2C-R is relatively weaker than that of Mo_2C-R (magenta line, Fig. 3). A higher intensity indicates a higher content of Mo_2C for the porous Mo_2C-R compared to HMo-Mo_2C-R and LMo-Mo_2C-R. This correlates well with their HER activity and suggests Mo_2C phase is responsible for the catalytic activity towards hydrogen evolution.

To understand various processes during HER, electrochemical impedance spectroscopy (EIS) was carried out under different overpotentials. At $\eta = 0$–100 mV, Bode plots suggest a one-time-constant process for both LMo-Mo_2C-R (Fig. S6b) and Mo_2C-R (Fig. 6b). Nyquist plot also confirms this behaviour of Mo_2C-R, indicated by one semi-circle, as shown in Fig. 6a. Interestingly, when the overpotential is increased up to $\eta = 150$ mV and 200 mV, it is found that a linear part emerges at high frequency which is associated with the transport process [51]. Low-frequency region is highly potential-dependent by comparing Fig. 6c with 6d, suggesting a charge-transfer process. Hence, a model of a R_s representing the ohmic resistance of electrolyte and all contact resistances, in series with a Constant Phase Element (CPE) that is in parallel with a Warburg impedance and a charge-transfer resistance (R_{ct}) (see the model in Fig. S6), is applied and the R_{ct} and Warburg resistance (R_W) of the fitted results are presented in Table 1. As shown in Fig. 6d, it is clear that Mo_2C-R (R_{ct}, 1.4 Ω; R_W, 3.9 Ω) shows a faster charge-transfer and diffusion process than LMo-Mo_2C-R (R_{ct}, 4.9 Ω; R_W, 6.9 Ω) at $\eta = 200$ mV. In contrast, HMo-Mo_2C-R exhibits one-time-constant behaviour at all potentials applied (Fig. S6a).

At low current density, where mass transport is negligible, Tafel analysis can be applied to analyse the reaction mechanism. The detailed Tafel slopes and exchange current densities are summarized in Table 1. The Tafel slopes of 66 mV dec^{-1} and 58 mV dec^{-1} (*IR* drop corrected) for Mo_2C-R were observed, which is comparable to the previously reported values of 55 mV dec^{-1} for Mo_2C-CNT [36] and 62.7 mV dec^{-1} for MoSoy/RGO [37]. Generally, to convert protons to H_2, three elementary reaction steps are involved [52], Volmer: $H^+ + e^- \rightarrow H_{ad}$ (1), Heyrovsky: $H_{ad} + H^+ + e^- \rightarrow H_2$ (2) and Tafel: $H_{ad} + H_{ad} \rightarrow H_2$ (3). Molecular hydrogen can be produced when reaction (1) is combined with reaction (2), or reaction (3). If the Volmer step is the rate-determining step, it invokes a Tafel slope of 120 mV dec^{-1}. If the Heyrovsky or Tafel reaction is the rate-determining step, it gives a Tafel slope of ~40 mV dec^{-1} or ~30 mV dec^{-1}, respectively. In our study, a Tafel slope of ~58 mV dec^{-1} or Mo_2C-R implies the Volmer–Heyrovsky mechanism. By extrapolating the linear part of the potential-log|*j*| plot at $\eta = 0$ (Fig. S5), the exchange current density can be obtained (Table 1). In contrast to commercial Mo_2C, the exchange current densities of all the as-synthesized nano-rod catalysts are found in the order of magnitude of ~10^{-2} mA cm^{-2} and are comparable to the hybrid Mo_2C–CNT [36], 1.4×10^{-2} mA cm^{-2} and MoSoy/RGO, 3.7×10^{-2} mA cm^{-2} [37]. These values are higher than molybdenum disulphide [53–55], suggesting its promising activity towards HER as a standalone catalyst.

Table 1
Tafel slope *b*, exchange current density j_o in 0.5 M H_2SO_4.

	b (mV dec^{-1})	j_o (mA cm^{-2})	R_{ct} @ $\eta = 200$ mV (Ω)	R_{Ws} @ $\eta = 200$ mV (Ω)
Mo_2C-R	58	3.3×10^{-2}	1.4	3.9
LMo-Mo_2C-R	70	3.1×10^{-2}	4.9	6.9
HMo-Mo_2C-R	74	1.5×10^{-2}	11.6	–
Commercial Mo_2C	73	1.4×10^{-3}	–	–
20 wt.% Pt/C	32	0.62	–	–

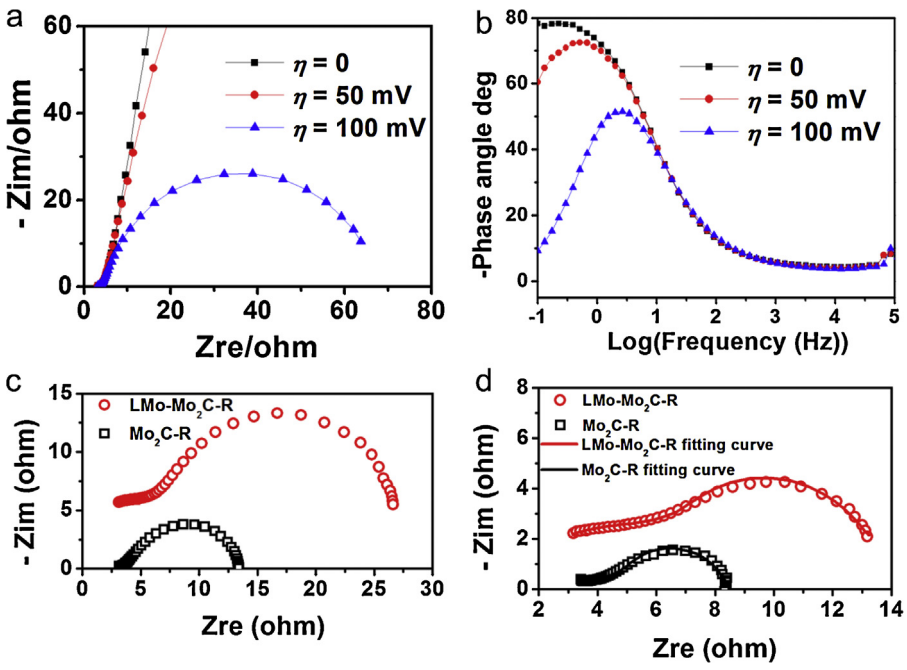

Fig. 6. EIS curves in 0.5 M H_2SO_4: (a) Nyquist plot and (b) Bode plot of Mo_2C-R; (c) Nyquist plots of LMo-Mo_2C-R and Mo_2C-R at $\eta = 150$ mV; (d) Nyquist plots of LMo-Mo_2C-R, Mo_2C-R and their fitting results at $\eta = 200$ mV.

Stability is a key factor for evaluating a catalyst. Long-term stability was tested by cycling potential from −0.24 to 0 V *vs.* RHE. As shown in Fig. 7, there is a slight decay of current density in the first 1000 cycles, but it retains its activity in the second 1000 cycles, which demonstrates an excellent cycling life in acidic environment.

Few catalysts can be employed in both acid and alkaline media. Noble metal Pt is one of them. Previously, non-noble commercial Mo_2C was proposed as a catalytic candidate for hydrogen evolution in basic conditions by Hu et al. [13]. In this study, we also examined the HER activity of the porous Mo_2C nano-rod in high pH condition. It was observed that the current density reaches ~30 mA cm^{-2} at $\eta = 200$ mV as shown in Fig. 8, exhibiting an advantageous performance over commercial Mo_2C (0.5 mA cm^{-2} at $\eta = 200$ mV). However, it still lacks competition compared to Pt catalyst, especially in view of the onset potential; ~67 mV *vs.* nearly zero for Pt in Fig. 8, which implies that a higher overpotential is needed to drive HER. Nickel as a cheap metal has been widely explored for hydrogen evolution in concentrated alkaline media. The low overpotential, high exchange current density [56,57], especially in nano-powder [16] make nickel a competitive catalyst for HER. Therefore, Ni is incorporated into the Mo_2C nano-rods to form the Ni supported Mo_2C-R, denoted Ni-Mo_2C-R (Fig. S7). With increased loading of Ni, the onset potential decreases. In particular, when the loading amount is up to 30 wt.%, the onset potential is similar to that of Pt in Fig. 8. However, it is compromised by higher overpotential at high cathodic current density region. The Tafel slope *b* and current densities are summarized in Table 2, where Mo_2C-R shows a Tafel slope of 45 mV dec^{-1} with the exchange current density of 1.1×10^{-2} mA cm^{-2}, similar to its performance in acidic media. It is also observed that the exchange current density increases with the

Table 2
Tafel slope *b*, exchange current density j_o in 1 M KOH.

	b (mV dec^{-1})	j_o (mA cm^{-2})
Mo_2C-R	45	1.1×10^{-2}
3 wt.% Ni-Mo_2C-R	55	3.9×10^{-2}
10 wt.% Ni-Mo_2C-R	73	0.14
30 wt.% Ni-Mo_2C-R	49	0.27

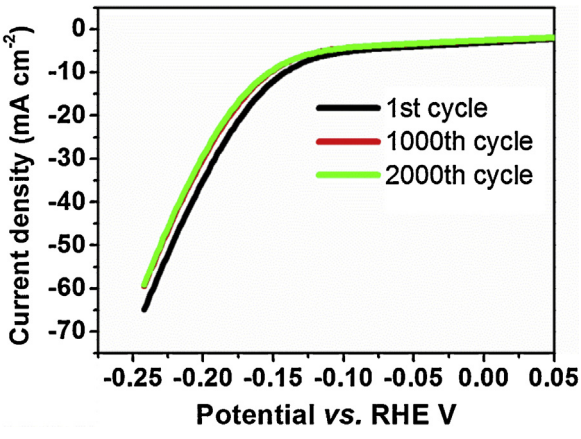

Fig. 7. Stability test of Mo_2C-R in 0.5 M H_2SO_4, scanning rate: 100 mV s^{-1}.

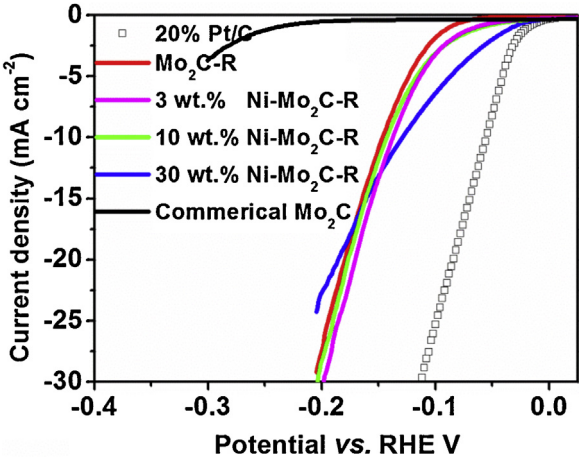

Fig. 8. Polarization curves of various catalysts in 1 M KOH solution.

increased loading of Ni. However, the Tafel slope does not follow the same tendency. In the perspectives of elementary steps of hydrogen evolution, it is possible that Ni promotes the adsorption of H species, compared to pure Mo_2C-R due to its strong bond to H [11]. Thus, it could explain the increased exchange current density and decreased onset potential. On the other hand, it hampers the H_{ad} or molecular H_2 release from the active sites, and furthermore, high loading of Ni may occupy part of the active sites or the pathways for H^+ to access Mo_2C-R on the surface (Fig. S7b). This could give explanation to the decreased current density when high content of Ni was incorporated and also expounds the changes of Tafel slope because of the ambivalent effects invoked by Ni, However, the detailed mechanism of the decreased onset potential and degraded performance at high current density is not fully understood at this stage and further experiments are needed.

4. Conclusions

In summary, we have successfully synthesized Mo_2C nano-rods through facile carburization of anilinium molybdate. The excellent electrocatalytic performance towards hydrogen evolution was observed in both acidic (32 mA cm^{-2}, at $\eta = 200$ mV) and alkaline media (30 mA cm^{-2}, at $\eta = 200$ mV) as a non-noble metal catalyst. Tafel slopes of 58 mV dec^{-1} in acidic medium and 45 mV dec^{-1} in alkaline medium suggest a Volmer–Heyrovsky rate-determining mechanism. The high performance results from the high conductivity and well-defined, porous morphology. Incorporation of Ni onto Mo_2C nano-rods reveals that Mo_2C lacks adsorptive bonding to H species at low overpotentials compared to metal Ni, thus causing high onset potential. More importantly, the incorporation of Ni onto Mo_2C nano-rods reveals the discrepant nature of metals (*e.g.* Ni) and compounds (*e.g.* Mo_2C) for hydrogen evolution. It illuminates the possible ways for further improvement of the performance by incorporating Ni into carbide to form nickel molybdenum carbide complex.

Acknowledgements

We acknowledge financial support from the academic research fund AcRF tier 1 (M4011020 RG8/12) Ministry of Education, Singapore and competitive research program (2009 NRF-CRP 001-032), National Research Foundation, Singapore.

Appendix A. Supplementary data

Supplementary material related to this article can be found, in the online version, at http://dx.doi.org/10.1016/j.apcatb.2014.02.020.

References

[1] A. Le Goff, V. Artero, B. Jousselme, P.D. Tran, N. Guillet, R. Métayé, A. Fihri, S. Palacin, M. Fontecave, Science 326 (2009) 1384–1387.
[2] M.S. Dresselhaus, I.L. Thomas, Nature 414 (2001) 332–337.
[3] J.A. Turner, Science 305 (2004) 972–974.
[4] W.-F. Chen, K. Sasaki, C. Ma, A.I. Frenkel, N. Marinkovic, J.T. Muckerman, Y. Zhu, R.R. Adzic, Angew. Chem. Int. Ed. 51 (2012) 6131–6135.
[5] Y. Yan, L. Zhang, X. Qi, H. Song, J.-Y. Wang, H. Zhang, X. Wang, Small 8 (2012) 3350–3356.
[6] E. Antolini, Appl. Catal. B: Environ. 74 (2007) 337–350.
[7] E. Antolini, Appl. Catal. B: Environ. 74 (2007) 324–336.
[8] A. Serov, C. Kwak, Appl. Catal. B: Environ. 90 (2009) 313–320.
[9] D.J. Evans, C.J. Pickett, Chem. Soc. Rev. 32 (2003) 268–275.
[10] A. Volbeda, J.C. Fontecilla-Camps, Dalton Trans. (2003) 4030–4038.
[11] B. Hinnemann, P.G. Moses, J. Bonde, K.P. Jørgensen, J.H. Nielsen, S. Horch, I. Chorkendorff, J.K. Nørskov, J. Am. Chem. Soc. 127 (2005) 5308–5309.
[12] Z. Wu, B. Fang, A. Bonakdarpour, A. Sun, D.P. Wilkinson, D. Wang, Appl. Catal. B: Environ. 125 (2012) 59–66.
[13] H. Vrubel, X. Hu, Angew. Chem. Int. Ed. 51 (2012) 12703–12706.
[14] F. Harnisch, G. Sievers, U. Schröder, Appl. Catal. B: Environ. 89 (2009) 455–458.
[15] F. Harnisch, U. Schröder, M. Quaas, F. Scholz, Appl. Catal. B: Environ. 87 (2009) 63–69.
[16] J.R. McKone, B.F. Sadtler, C.A. Werlang, N.S. Lewis, H.B. Gray, ACS Catal. (2012) 166–169.
[17] H. Vrubel, D. Merki, X. Hu, Energy Environ. Sci. 5 (2012) 6136–6144.
[18] D. Merki, X. Hu, Energy Environ. Sci. 4 (2011) 3878–3888.
[19] D. Merki, S. Fierro, H. Vrubel, X. Hu, Chem. Sci. 2 (2011) 1262–1267.
[20] D. Merki, H. Vrubel, L. Rovelli, S. Fierro, X. Hu, Chem. Sci. 3 (2012) 2515–2525.
[21] T.-W. Lin, C.-J. Liu, J.-Y. Lin, Appl. Catal. B: Environ. 134–135 (2013) 75–82.
[22] T.F. Jaramillo, K.P. Jørgensen, J. Bonde, J.H. Nielsen, S. Horch, I. Chorkendorff, Science 317 (2007) 100–102.
[23] A.B. Laursen, S. Kegnaes, S. Dahl, I. Chorkendorff, Energy Environ. Sci. 5 (2012) 5577–5591.
[24] J.N. Coleman, M. Lotya, A. O'Neill, S.D. Bergin, P.J. King, U. Khan, K. Young, A. Gaucher, S. De, R.J. Smith, I.V. Shvets, S.K. Arora, G. Stanton, H.-Y. Kim, K. Lee, G.T. Kim, G.S. Duesberg, T. Hallam, J.J. Boland, J.J. Wang, J.F. Donegan, J.C. Grunlan, G. Moriarty, A. Shmeliov, R.J. Nicholls, J.M. Perkins, E.M. Grieveson, K. Theuwissen, D.W. McComb, P.D. Nellist, V. Nicolosi, Science 331 (2011) 568–571.
[25] G. Eda, H. Yamaguchi, D. Voiry, T. Fujita, M. Chen, M. Chhowalla, Nano Lett. 11 (2011) 5111–5116.
[26] Y. Li, H. Wang, L. Xie, Y. Liang, G. Hong, H. Dai, J. Am. Chem. Soc. 133 (2011) 7296–7299.
[27] E.G.S. Firmiano, M.A.L. Cordeiro, A.C. Rabelo, C.J. Dalmaschio, A.N. Pinheiro, E.C. Pereira, E.R. Leite, Chem. Commun. 48 (2012) 7687–7689.
[28] Y. Yan, B. Xia, X. Qi, H. Wang, R. Xu, J.-Y. Wang, H. Zhang, X. Wang, Chem. Commun. 49 (2013) 4884–4886.
[29] X. Bian, J. Zhu, L. Liao, M.D. Scanlon, P. Ge, C. Ji, H.H. Girault, B. Liu, Electrochem. Commun. 22 (2012) 128–132.
[30] Y. Yan, X. Ge, Z. Liu, J.-Y. Wang, J.-M. Lee, X. Wang, Nanoscale 5 (2013) 7768–7771.
[31] C. Shi, A. Zhang, X. Li, S. Zhang, A. Zhu, Y. Ma, C. Au, Appl. Catal. A: Gen. 431–432 (2012) 164–170.
[32] A.C. Lausche, J.A. Schaidle, L.T. Thompson, Appl. Catal. A: Gen. 401 (2011) 29–36.
[33] J. Han, J. Duan, P. Chen, H. Lou, X. Zheng, H. Hong, ChemSusChem 5 (2012) 727–733.
[34] J.A. Schaidle, A.C. Lausche, L.T. Thompson, J. Catal. 272 (2010) 235–245.
[35] L. Liao, S. Wang, J. Xiao, X. Bian, Y. Zhang, M.D. Scanlon, X. Hu, Y. Tang, H.H. Girault, B. Liu, Energy Environ. Sci. (2013), http://dx.doi.org/10.1039/C3EE42441C.
[36] W.F. Chen, C.H. Wang, K. Sasaki, N. Marinkovic, W. Xu, J.T. Muckerman, Y. Zhu, R.R. Adzic, Energy Environ. Sci. 6 (2013) 943–951.
[37] W.-F. Chen, S. Iyer, S. Iyer, K. Sasaki, C.-H. Wang, Y. Zhu, J.T. Muckerman, E. Fujita, Energy Environ. Sci. 6 (2013) 1818–1826.
[38] Q. Gao, C. Zhang, S. Xie, W. Hua, Y. Zhang, N. Ren, H. Xu, Y. Tang, Chem. Mater. 21 (2009) 5560–5562.
[39] Q. Gao, S. Wang, H. Fang, J. Weng, Y. Zhang, J. Mao, Y. Tang, J. Mater. Chem. 22 (2012) 4709–4715.
[40] S. Toksoz, H. Acar, M.O. Guler, Soft Matter 6 (2010) 5839–5849.
[41] W. Lasocha, J. Jansen, H. Schenk, J. Solid State Chem. 117 (1995) 103–107.
[42] K. Oshikawa, M. Nagai, S. Omi, J. Phys. Chem. B 105 (2001) 9124–9131.
[43] B. Brox, I. Olefjord, Surf. Interface Anal. 13 (1988) 3–6.
[44] V. Singh, D. Joung, L. Zhai, S. Das, S.I. Khondaker, S. Seal, Prog. Mater. Sci. 56 (2011) 1178–1271.
[45] M.S. Dresselhaus, A. Jorio, M. Hofmann, G. Dresselhaus, R. Saito, Nano Lett. 10 (2010) 751–758.
[46] M.-L. Frauwallner, F. López-Linares, J. Lara-Romero, C.E. Scott, V. Ali, E. Hernández, P. Pereira-Almao, Appl. Catal. A: Gen. 394 (2011) 62–70.
[47] H.A. Becerril, J. Mao, Z. Liu, R.M. Stoltenberg, Z. Bao, Y. Chen, ACS Nano 2 (2008) 463–470.
[48] S.P. Jiang, L. Liu, K.P. Ong, P. Wu, J. Li, J. Pu, J. Power Sources 176 (2008) 82–89.
[49] W. Zhou, Z. Shao, R. Ran, P. Zeng, H. Gu, W. Jin, N. Xu, J. Power Sources 168 (2007) 330–337.
[50] J.K. Nørskov, T. Bligaard, A. Logadottir, J.R. Kitchin, J.G. Chen, S. Pandelov, U. Stimming, J. Electrochem. Soc. 152 (2005) J23–J26.
[51] H. Vrubel, T. Moehl, M. Gratzel, X. Hu, Chem. Commun. 49 (2013) 8985–8987.
[52] Z. Chen, D. Cummins, B.N. Reinecke, E. Clark, M.K. Sunkara, T.F. Jaramillo, Nano Lett. 11 (2011) 4168–4175.
[53] D. Kong, H. Wang, J.J. Cha, M. Pasta, K.J. Koski, J. Yao, Y. Cui, Nano Lett. 13 (2013) 1341–1347.
[54] J. Kibsgaard, Z. Chen, B.N. Reinecke, T.F. Jaramillo, Nat. Mater. 11 (2012) 963–969.
[55] J. Bonde, P.G. Moses, T.F. Jaramillo, J.K. Norskov, I. Chorkendorff, Faraday Discuss. 140 (2009) 219–231.
[56] J.Y. Huot, M.L. Trudeau, R. Schulz, J. Electrochem. Soc. 138 (1991) 1316–1321.
[57] J.Y. Huot, L. Brossard, Int. J. Hydrogen Energy 12 (1987) 821–830.